The modelled surface mass balance of the Antarctic Peninsula at 5.5 km horizontal resolution.

van Wessem, J.M.; Ligtenberg, S.R.M.; Reijmer, C.H.; van de Berg, W.J.; van den Broeke, M.R.; Thomas, E.R.; Barrand, Nicholas E.; Turner, J.; Wuite, J.; Scambos, T.A.; van Meijgaard, E.

DOI:
10.5194/tcd-9-5097-2015

Manuscript prepared for The Cryosphere
with version 4.2 of the LaTeX class copernicus.cls.
Date: 27 August 2015

The modelled surface mass balance of the Antarctic Peninsula at 5.5 km horizontal resolution

J. M. van Wessem[1], S. R. M. Ligtenberg[1], C. H. Reijmer[1], W. J. van de Berg[1], M. R. van den Broeke[1], N. E. Barrand[2], E. R. Thomas[3], J. Turner[3], J. Wuite[4], T. A. Scambos[5], and E. van Meijgaard[6]

[1]Institute for Marine and Atmospheric Research Utrecht, Utrecht University, Utrecht, the Netherlands
[2]School of Geography, Earth and Environmental Sciences, University of Birmingham, UK
[3]British Antarctic Survey, Cambridge, UK
[4]ENVEO IT GmbH, Innsbruck, Austria
[5]National Snow and Ice Data Center, University of Colorado, Boulder CO, USA
[6]Royal Netherlands Meteorological Institute, De Bilt, the Netherlands

Correspondence to: J. M. van Wessem (j.m.vanwessem@uu.nl)

Abstract. This study presents a high-resolution (∼5.5 km) estimate of Surface Mass Balance (SMB) over the period 1979–2014 for the Antarctic Peninsula (AP), generated by the regional atmospheric climate model RACMO2.3 and a Firn Densification Model (FDM). RACMO2.3 is used to force the FDM, which calculates processes in the snowpack, such as meltwater percolation, refreezing and runoff. We evaluate model output with 132 in-situ SMB observations and discharge rates from 6 glacier drainage basins, and find that the model realistically simulates the strong spatial variability in precipitation, but that significant biases remain as a result of the highly complex topography of the AP. It is also clear that the observations significantly underrepresent the high-accumulation regimes.

The SMB map reveals large accumulation gradients, with precipitation rates above 3000 $\mathrm{mm\ w.e.\ y^{-1}}$ over the western AP (WAP) and below 500 $\mathrm{mm\ w.e.\ y^{-1}}$ on the eastern AP (EAP), not resolved by coarser data-sets such as ERA-Interim. The other SMB components are one magnitude smaller, with drifting snow sublimation the largest ablation term removing up to 100 $\mathrm{mm\ w.e.\ y^{-1}}$ of mass. Snowmelt is widespread over the AP, reaching 500 $\mathrm{mm\ w.e.\ y^{-1}}$ towards the northern ice shelves, but the meltwater mostly refreezes. As a result runoff fluxes are low, but still considerable (200 $\mathrm{mm\ w.e.\ y^{-1}}$) over the Larsen (B/C), Wilkins and George VI ice shelves. The average AP ice sheet integrated SMB, including ice shelves (an area of $4.1{\cdot}10^5$ km^2), is estimated at 351 $\mathrm{Gt\ y^{-1}}$ with an interannual variability of 58 $\mathrm{Gt\ y^{-1}}$, which is dominated by precipitation (PR) (365 ± 57 Gt y^{-1}). The WAP ($2.4{\cdot}10^5$ km^2) SMB (276 ± 47 Gt y^{-1}), where PR is large (276 ± 47 Gt y^{-1}), dominates over the EAP ($1.7{\cdot}10^5$ km^2) SMB (75 ± 11 Gt y^{-1}) and PR (84 ± 11 Gt y^{-1}). Total sublimation is 11 ± 2 Gt y^{-1} and meltwater runoff into the ocean is 4 ± 4 Gt y^{-1}. There are no significant trends

in any of the AP SMB components, except for snowmelt that shows a significant decrease over the last 36 years (–0.36 $\mathrm{Gt\ y^{-2}}$).

1 Introduction

The Antarctic Peninsula (AP) is one of the most rapidly changing regions on earth (Turner et al., 2005). Over the last 50 years, the AP has experienced a warming of 3 K that is higher than in any other region on earth (Bromwich et al., 2012), and has increasingly contributed to global sea level rise (Shepherd et al., 2012; Wouters et al., 2015). In addition, the AP is the only region of Antarctica that is warm enough for widespread surface melt to occur, which has increased unprecedentedly over the past 1000 years (Abram et al., 2013). Likely as a result of the increased melt rates, many of the ice shelves that fringe the AP have (partly) disintegrated in recent years (Cook et al., 2005), potentially due to hydrofracturing of surface crevasses (Vaughan et al., 2003; Van den Broeke, 2005). In combination with warmer ocean currents melting the ice shelves from below (Pritchard et al., 2012; Wouters et al., 2015), the ice shelves lose their buttressing effect (Dupont and Alley, 2005), accelerating the AP glaciers flowing into the ice shelves, and raising sea level (Rignot et al., 2011; Shepherd et al., 2012; Scambos et al., 2000). Increased snowfall could compensate these effects on sea level (Davis et al., 2005). In order to quantify the mass changes of the AP and the associated sea level rise, an accurate estimate of the AP surface mass balance is essential.

The surface mass balance (SMB in $\mathrm{mm\ w.e.\ y^{-1}}$) is defined as the sum of all mass fluxes towards/away from the ice sheet surface:

$$\mathrm{SMB} = \int_{\mathrm{year}} (\mathrm{PR} - \mathrm{SU_s} - \mathrm{SU_{ds}} - \mathrm{ER_{ds}} - \mathrm{RU}) dt \tag{1}$$

where PR represents total precipitation (snowfall plus rain), SU surface ($\mathrm{SU_s}$) plus drifting snow ($\mathrm{SU_{ds}}$) sublimation, $\mathrm{ER_{ds}}$ drifting snow erosion and RU meltwater runoff, the amount of liquid water (melt and rain) that is not retained or refrozen in the snowpack. The mean area averaged SMB of the AP is 6 times larger than that of the total Antarctic ice sheet (AIS) (Van Lipzig et al., 2004), and AP melt rates are also relatively large due to its northerly location (Barrand et al., 2013). The high accumulation rates are a result of the AP acting as an efficient mountain barrier, forcing large amounts of orographic precipitation along its windward slopes.

Measuring AP SMB is a complicated task, as the high precipitation rates and the steep mountainous (and inaccessible) terrain leave large regions devoid of observational data; most observations are located in relatively dry areas and/or over the flat ice shelves which are easily accessible (Favier et al., 2013). Available observations have identified a doubling of snowfall over the WAP since 1850 (Thomas et al., 2008), an increase in SMB over the last 50 years (Peel, 1992), or a large spatial variability of the SMB (Turner et al., 2002). To solve the limited coverage of these observations remote sensing techniques are pivotal. Remote sensing techniques, such as radar backscatter to identify melt

episodes (Barrand et al., 2013) or satellite products like the Gravity Recovery and Climate Experiment (GRACE; Tapley et al., 2004), often don't resolve the small scale features of the AP SMB. Other methods, such as using ice discharge estimates to calculate the mass balance of the ice sheet, or satellite altimetry to measure thickness changes, need detailed SMB fields (Rignot et al., 2011; Mouginot et al., 2012; Wuite et al., 2015), or require a correction for firn processes (Gunter et al., 2009), which is dependent on the SMB. Therefore, for a realistic mass balance estimate, continuous SMB fields from climate model simulations are necessary.

Regional atmospheric climate models (RCMs) realistically simulate the climate and SMB of the larger glaciated regions, such as Greenland (Fettweis, 2007; Van Angelen et al., 2013) and Antarctica (Bromwich, 2004; Lenaerts et al., 2012b). Moreover, RCMs have, in combination with a Firn Densification Model (FDM, Ligtenberg et al., 2011), been used to simulate the interaction of the snowpack with the atmosphere and a changing climate (Ligtenberg et al., 2014; Kuipers Munneke et al., 2015), providing detailed information about meltwater percolation, refreezing and the stability of ice shelves (Kuipers Munneke et al., 2014).

The SMB and climate of the AP have been simulated before, at a relatively high (14 km) resolution, but for a short timespan (6 years) (Van Lipzig et al., 2004). Higher resolution simulations have also been performed, but without a high-resolution snow-routine (Bromwich, 2004; King et al., 2015). Recently, the regional atmospheric climate model RACMO2.3 was used at a horizontal resolution of 5.5 km to simulate the SMB of Patagonia (Lenaerts et al., 2014). In this study we use the same model and resolution to simulate the SMB of the AP for 1979–2014, the period for which reliable forcing data is available, coupling it to a FDM to calculate processes in the firnpack and, eventually, runoff. We discuss the SMB and its components, with a particular focus on meltwater and precipitation. We present the model and the observations used in Sect. 2, and evaluate the modelled SMB with in-situ observations and discharge estimates in Sect. 3. In Sect. 4, we discuss gridded climate maps of SMB and its components, and discuss spatial and temporal variability. Finally, we present a discussion of the results and conclusions in Sects. 5 and 6.

2 Data and Methods

2.1 Regional Atmospheric Climate Model RACMO2.3

The Regional Atmospheric Climate Model RACMO2.3 combines the dynamics package of the High Resolution Limited Area Model (HIRLAM) (Undén et al., 2002) with the physics package of the European Centre for Medium-range Weather Forecasts (ECMWF) Integrated Forecast System (IFS). RACMO2.3 has been adapted for use over the large ice sheets of Greenland and Antarctica: it includes a multi-layer snow model to calculate melt, percolation, refreezing and runoff of liquid water (Ettema et al., 2010); a prognostic scheme to calculate surface albedo based on snow grain size (Kuipers Munneke et al., 2011); and a routine that simulates the interaction of drifting snow

with the surface and the lower atmosphere (Lenaerts et al., 2012a). ERA-Interim re-analysis data with 6-hourly resolution from January 1979 to December 2014 (Dee et al., 2011) are used to force the model at the lateral atmospheric boundaries as well as at the lower ocean boundaries by prescribing sea ice fraction and sea surface temperatures. The model domain interior (Fig. 1) is allowed to evolve freely and a model time step of 2 minutes is used.

RACMO2.3 is a hydrostatic model, that we run at a horizontal resolution of $\sim$5.5 km and 40 vertical levels. At this resolution we assume the assumption of hydrostatic balance to hold, a assumption that is justified to some extent by earlier studies (Lenaerts et al., 2014; Van Wessem et al., 2015), although a non-hydrostatic model version will likely further improve the model output in terms of better resolved processes over sloping surfaces, such as foehn and katabatic winds that influence (drifting snow) sublimation and snowmelt fluxes (Cassano and Parish, 2000). The surface topography is based on a combination of the 100 m Digital Elevation Model (DEM) from Cook et al. (2012) and the 1 km DEM from Bamber and Gomez-Dans (2009). The ice sheet mask is kept constant through the simulation, and includes the (former) Larsen B and Larsen A ice shelves. All integrated SMB estimates use basins number 24–27 from the basin definition from Zwally et al. (2012), and include Larsen B, but for calculations (e.g. yearly averages) after its disintegration (2003), Larsen B is excluded. For 1979–2014 averages the full ice sheet mask including Larsen B is used. For further details of the model the reader is referred to Van Wessem et al. (2015).

The model is initialised on January 1st, 1979, with the atmospheric state and sea surface boundary conditions adopted from ERA-Interim reanalysis. The initial firnpack of the AP is inferred from a simulation with an offline firn densification model (FDM, Ligtenberg et al., 2011), which was driven by an earlier climatological simulation of the AP by RACMO2.3, largely comparable to the one used in this study. Runoff estimates are taken from the FDM, which was forced by RACMO2.3: the other SMB components are directly from RACMO2.3.

2.2 Firn Densification Model

The Firn Densification Model (FDM) is a high-resolution version (in the vertical) of the snow model that is interactively coupled to RACMO2.3. It is a single column time-dependent model that describes the evolution of the firn layer. It calculates firn density, temperature and liquid water content evolution based on forcing at the surface by RACMO2.3 variables at 3 hourly resolution: surface temperature, accumulation and wind speed. Surface meltwater percolates into the model firn layer, where it can refreeze, be stored or percolate further down. The retention of meltwater is based on the 'tipping-bucket' method (i.e. liquid water is stored in the first available layer and transported downwards only when it exceeds capillary forces). Liquid water that reaches the bottom of the firn layer and can neither be refrozen or stored will be removed as runoff (RU in Eq. 1). We have coupled the FDM offline to RACMO2.3, having found no significant differences due to e.g. the interaction of the atmosphere with subsurface processes in the snow column. A detailed analysis of subsurface

processes is beyond the scope of this study; here we focus on the integrated mass budget and the SMB. More details on the FDM can be found in Ligtenberg et al. (2011).

2.3 Observational data

2.3.1 In-situ observations

We evaluate modelled SMB using 132 in-situ observations, originating from various sources and methods: e.g. ice cores, stake arrays and bomb horizons (Fig. 1) (Turner et al., 2002; Favier et al., 2013; Scambos et al., 2014). Included in these data are five unpublished in-situ observations from high elevations; obtained from a shallow ice core, sonic snow height measurements and camera observations of a snow stake over time (T.A. Scambos, personal communication, 2014). Also included are six ice core accumulation records: James Ross Island (Aristarain et al., 2004), Gomez (Thomas et al., 2008), two cores from Dyer Plateau, one to the east of the ice divide (Thompson et al., 1994), one to the west of the ice divide (Arthern et al., 2010, E.R. Thomas, unpublished, 2015), Bryan Coast and Ferrigno (E.R. Thomas, unpublished, 2015). These records are additionally used to assess model interannual variability in Sect. 3.2.

We compare modelled SMB with in-situ observations only for overlapping time periods, when available. When observations date from before 1979, or when the time of measurement is not known, they are compared with the climatological (1979–2014) modelled SMB. Only 38 SMB observations have an observation length >5 years and these are used for model evaluation in Sect. 4.

2.3.2 Discharge estimates

We evaluate modelled SMB using 1995 pre-collapse discharge (D) estimates of six Larsen B outlet glaciers in the northeastern AP. We assume these to be in balance ($\mathrm{SMB} - \mathrm{D} = 0$) , as the data comes from well before the significant thinning and retreat of the Larsen B ice shelf, that culminated in its break-off in 2002 (Wuite et al., 2015); we exclude basins that are too small to be resolved by the model resolution, or were not in balance. This leaves six basins: Starbuck, Flask, Leppard, Crane, Jorum and Hektoria-Green, shown in Fig. 1. Assuming balance of these basins, a comparison with the climate average SMB for 1979–2014 is justified, and we directly compare discharge with RACMO2.3 SMB for this period.

3 Results: Model evaluation

3.1 In-situ observations

Figure 2 compares modelled (red) and observed (black) SMB for the locations of the in-situ observations (averaged in elevation bins). As many SMB observations are clustered, i.e. mostly located on the ice shelves and locations of relatively low accumulation, we have binned the observations in

eleven surface elevation bins, selected such that they span at least ∼75 m in elevation and contain at least 10 SMB data points. The bins are arranged from left to right in eight western AP (WAP) bins (W1 – W8), one bin for the spine (S) and two bins for the eastern AP (EAP; E1 – E2). Figure 2 shows that the model and the observations show relatively constant SMB values for the WAP and the EAP ($<$1000 $\mathrm{mm\ w.e.\ y^{-1}}$), and a pronounced peak in SMB over the spine. Variability between the different bins is caught well and simulated SMB is always within the standard deviation of the observations. For bins W2, W6 and W7 there is a slightly larger discrepancy with the observations. To explain this, we calculated the average of all model grid points within the respective bins (green points). These averages are considerably higher than both the observed and modelled values, showing that the observations are biased towards regions of low accumulation.

Figure 3a presents the direct correlation between the model and the observations, both for the individual locations as for the eleven elevation bins. The SMB over the AP is highly variable and modelled SMB is poorly correlated with the individual observations (r^2= 0.25, rc = 0.46), although the average bias is low (bias = 28.4 $\mathrm{mm\ w.e.\ y^{-1}}$). The binned averages strongly improve the correlation (r^2 = 0.8) and the slope (rc = 0.97), demonstrating that larger-scale spatial variability is generally well simulated. The EAP SMB is well simulated, especially the low SMB over the ice shelves, even though few EAP observations are available. For the WAP, the model overestimates the relatively dry SMB locations (George VI ice shelf and southern Palmer Land), while underestimating the wetter locations (coastal zones). This is likely related to an insufficient representation of orographic precipitation at 5.5 km, both due too simple cloud physics (e.g. precipitation falls to the surface instantly, and is not transported across grid-boxes), the model being hydrostatic, and the remaining underestimation of the surface slope, as e.g. George VI ice shelf is in the precipitation shadow of the relatively high Alexander Island. The model does simulate the peak in SMB (∼2000 $\mathrm{mm\ w.e.\ y^{-1}}$) of the northern spine bin (containing WAP and EAP observations $>$1500 m elevation), despite the few observations and the very large spatial variability.

Figures 2 and 3a clearly present the main advantage of the high-resolution SMB product over low-resolution products such as the ERA-Interim re-analysis (Dee et al., 2011). Even though the re-analysis captures the SMB at the middle elevation bins reasonably well, it lacks the ability to resolve the steep SMB gradients, and the large SMB values at the higher elevations, as well as the low SMB over the WAP and EAP ice shelves. Another remarkable difference is the small spatial variability in ERA-Interim, compared to RACMO2.3 and the observations.

3.2 Interannual variability

Figure 4 shows yearly modelled (red) and observed (black) SMB at the location of six ice cores, suggesting that yearly modelled SMB is to a large extent representative of the observations. The model mainly underestimates the absolute SMB east and west of the ice divide at Dyer Plateau (Figs. 11c,d), where spatial variability is large, although for the western Dyer Plateau record the

modelled and observed variability matches relatively well, but both these records are very short. The records of Gomez, Bryan Coast and Ferrigno over the WAP, and James Ross Island over the EAP, match particularly well: the magnitude is simulated well by the model at these locations, and correlation coefficients are larger as well, although the model has difficulties in timing the SMB optima at the Gomez and James Ross ice cores. For James Ross Island this is likely related to the ice core being located on a small island with large elevation differences.

3.3 Discharge

We assessed modelled climatological SMB by comparing it to solid ice discharge estimates from glacier basins, for a time period when these were in approximate balance (pre-1995, Wuite et al., 2015). Figure 3b shows that modelled SMB matches the discharge estimates, especially for the smaller basins (Jorum, Starbuck and Flask). For the larger basins the representation is still generally good (bias $<$30%), especially considering the relatively small size of these basins (Fig. 1), and the large spatial variability along the northern AP mountain spine.

4 Results: Modelled SMB

4.1 Spatial variability

4.1.1 SMB components

Figure 5 presents average 1979–2014 AP SMB components (Eq. 1) and Fig. 6 the resulting SMB. Total precipitation (PR = snowfall + rainfall, Fig. 5a) dominates the AP SMB with values that are typically an order of magnitude larger than the other components, which is also the case for the whole AIS (Van Wessem et al., 2014a). PR shows large gradients (note the nonlinear scale in Figs. 5a and 6), with values ranging from $>$1000 $\mathrm{mm\ w.e.\ y^{-1}}$ on the western slopes and the adjacent ocean, towards low values ($<$300 $\mathrm{mm\ w.e.\ y^{-1}}$) on the eastern slopes and ice shelves. In particular the modelled precipitation rates in the northwestern AP are extreme with rates of up to 5000 $\mathrm{mm\ w.e.\ y^{-1}}$ on the lower windward slopes, equivalent to $\sim$15 m of snowfall each year. This makes the AP among the wettest regions (in terms of snowfall) on earth, in line with the high snowfall rates (3500 $\mathrm{mm\ w.e.\ y^{-1}}$) for Patagonia found with the same model (Lenaerts et al., 2014). These mountainous regions represent a steep barrier that is almost perpendicular to the strong circumpolar westerlies, causing very efficient orographically induced precipitation over the windward mountain slopes, and a strong precipitation shadow on the leeward slopes. These sharp gradients are widespread, especially in the WAP: for instance, although considerably lower, precipitation rates towards the south are high as well, varying from 2500 $\mathrm{mm\ w.e.\ y^{-1}}$ on the Elgar Uplands towards 1000–2000 $\mathrm{mm\ w.e.\ y^{-1}}$ on the western slopes of Palmer Land, with a distinct minimum over George VI ice shelf situated at the lee side of Alexander Island.

The second largest component is drifting snow sublimation (Fig. 5e), removing $\sim$50 $\mathrm{mm\ w.e.\ y^{-1}}$ of snowfall, peaking in regions of high wind speed (Van Wessem et al., 2015). $\mathrm{SU_{ds}}$ is smaller at high elevations and the (western) mountain slopes; here a stable surface temperature inversion favours surface deposition ($\mathrm{SU_s}$ = $\sim$–20 $\mathrm{mm\ w.e.\ y^{-1}}$, Fig. 5d). Surface sublimation ($\mathrm{SU_s}$ >0) mainly occurs over the flat ice shelves and the lower mountain slopes, removing $\sim$20 $\mathrm{mm\ w.e.\ y^{-1}}$ of snowfall. The erosion of drifting snow ($\mathrm{ER_{ds}}$) does not significantly contribute to the (integrated) SMB, but redistributes mass strongly on a local scale with snow divergence/convergence rates up to 100 $\mathrm{mm\ w.e.\ y^{-1}}$ on the AP slopes, closely following the topography. Snowmelt (M) is widespread below 2000 m a.s.l., showing large spatial variability, with maxima up to 500 $\mathrm{mm\ w.e.\ y^{-1}}$ over the northeastern ice shelves, and with decreasing M towards higher elevations and/or latitudes. Most meltwater refreezes or is retained in the snowpack, and only a fraction runs off into the ocean. This happens mainly over Larsen B and northern Larsen C ice shelves, but also over Wilkins and northern George VI ice shelves, with runoff (RU) fluxes up to 300 $\mathrm{mm\ w.e.\ y^{-1}}$. Over the lower slopes of the northwestern mountain range, where both PR and M are large, the model also simulates small amounts of runoff ($\sim$50 $\mathrm{mm\ w.e.\ y^{-1}}$).

4.1.2 SMB

Figure 6 presents the average modelled (1979–2014) SMB, together with the in-situ SMB observations with timespans >5 years. SMB is largely similar to PR (Fig. 5a), with large west-to-east gradients, and peak SMB values around the WAP coastal regions, with large spatial variability that is controlled by the orography. Although limited long-year in-situ observations are available, the modelled SMB patterns generally match with the observations: the large SMB values found only in a few observations are simulated well by the model, as well as the lower SMB values on the George VI and Larsen ice shelves. Only over the former Larsen B ice shelf there is a mismatch: here, simulated RU reaches its maximum, and modelled SMB is negative (up to –100 $\mathrm{mm\ w.e.\ y^{-1}}$). This negative SMB is not found in the pre-break-up observations, which show small but positive values. However, the model does agree that the minimum in SMB lies in this area. Furthermore, SMB is considerably overestimated at two locations on Adelaide Island and slightly eastwards.

4.2 Average integrated SMB

Table 1 summarises the integrated WAP (basins 24/25 from Zwally et al. (2012)), EAP (basins 26/27) and total (all basins) SMB values. The total AP SMB amounts to 351 $\mathrm{Gt\ y^{-1}}$, which is $\sim$20% of the total integrated SMB for the AIS as found in Van Wessem et al. (2014b), even though its area ($4.1 \cdot 10^5 \mathrm{km^2}$) is only 3% of the total AIS. The SMB over the WAP (276 $\mathrm{Gt\ y^{-1}}$) is considerably larger than that of the EAP (75 $\mathrm{Gt\ y^{-1}}$), although the larger area of the WAP ($2.4 \cdot \mathrm{km^2}$) compared to that of the EAP ($1.7 \cdot \mathrm{km^2}$) partly accounts for the difference. The large west-to-east differences are due to PR, that is 365 $\mathrm{Gt\ y^{-1}}$ in total, 281 $\mathrm{Gt\ y^{-1}}$ over the WAP and 84 $\mathrm{Gt\ y^{-1}}$ over the EAP. Of

PR, 97% is snowfall (363 $\mathrm{Gt\ y^{-1}}$); rainfall is small (3 $\mathrm{Gt\ y^{-1}}$). Total sublimation is 11 $\mathrm{Gt\ y^{-1}}$, dominated by $\mathrm{SU_{ds}}$ (9 $\mathrm{Gt\ y^{-1}}$). In contrast to the AIS, over the AP snowmelt is widespread and three times larger than the rest of the AIS combined (34 vs 11 $\mathrm{Gt\ y^{-1}}$ Van Wessem et al., 2014b). Most meltwater (and rainfall) refreezes in the snowpack (RF = 33 $\mathrm{Gt\ y^{-1}}$) but a small fraction runs off into the ocean (RU = 4 $\mathrm{Gt\ y^{-1}}$); most RU is present over the EAP, in particular over the Larsen B ice shelf (3 $\mathrm{Gt\ y^{-1}}$).

4.3 Temporal variability

4.3.1 Interannual variability

Figure 7 shows yearly average SMB values and the largest SMB components; for integrated values after 2003 we exclude Larsen B ice shelf. Total AP SMB (Fig. 7a) has an interannual variability of 58 $\mathrm{Gt\ y^{-1}}$ (15% of mean SMB, absolute values shown in Tab. 1) and shows no significant trends. Precipitation has a similar interannual variability of 57 $\mathrm{Gt\ y^{-1}}$. The most positive SMB year is 1989 with 445 $\mathrm{Gt\ y^{-1}}$, being significantly wetter than the driest year (1980, 246 $\mathrm{Gt\ y^{-1}}$), relatively a much larger difference than for the whole AIS (Lenaerts et al., 2012b), which is expected as over larger regions differences cancel out. Variability in sublimation and drifting snow sublimation is low, and comparable for the WAP and the EAP (1 $\mathrm{Gt\ y^{-1}}$). Of the SMB components (other than RU, that is small), the variability of M is the largest (15 $\mathrm{Gt\ y^{-1}}$, 45% of the mean), reaching its peak in 1992 (73 $\mathrm{Gt\ y^{-1}}$), and minima ($\sim$11 $\mathrm{Gt\ y^{-1}}$) in 1986 and 2014. EAP melt rates are higher by 3 $\mathrm{Gt\ y^{-1}}$ (relatively even higher as the area of the EAP is smaller than that of the WAP), but the timing of the maxima in M is similar. Simulated integrated AP snowmelt is lower than, but the variability and maxima are comparable to, the melt rates from Kuipers Munneke et al. (2012), (34 ± 15 Gt $\mathrm{y^{-1}}$ and 57 ± 21 Gt $\mathrm{y^{-1}}$, respectively) that were calculated with RACMO2.1 at 27 km horizontal resolution. Even though model physics have been updated and RACMO2.3 generally simulates less melt over the AIS (Van Wessem et al., 2014b), differences between both studies are explained by the use of a more sophisticated snowpack initialization in this study, and a different integration domain; i.e. in Kuipers Munneke et al. (2012) Larsen B is included for the whole period and the domain extends further south.

For all variables no significant trends are simulated, except for snowmelt (significance level >99%). Snowmelt has decreased by the same amount (–0.35 $\mathrm{Gt\ y^{-2}}$) over the WAP and the EAP, which is likely related to the significant and widespread cooling over most of the AP (Van Wessem et al., 2015). Runoff of meltwater is small but its variability is as high as its mean (4 $\mathrm{Gt\ y^{-1}}$), peak years reach values of up to 15 $\mathrm{Gt\ y^{-1}}$, following the peaks in M, 1992 and 1995 in particular. In contrast to M, RU over the WAP and EAP shows large differences. Despite the higher temperatures, a thick firnpack exists over the WAP, a result of the higher snowfall rates, refreezing most meltwater in the available pore space. Over the eastern ice shelves there is hardly any pore space present in the

firn and a larger fraction of meltwater runs off, especially over Larsen B ice shelf before 2003.

Figure 8 shows maps of SMB and M interannual variability. SMB variability (8a) shows no unexpected patterns for most of the domain, mostly following the regions of high absolute SMB. Relatively, SMB variability peaks over George VI, Larsen B and the northern part of Larsen C ice shelves (>40%). This is clearly related to RU (not shown), which in turn is controlled by snowmelt variability (Fig. 8b), that peaks towards the northern parts of the ice shelves. It is clear that dry regions, which experience significant melt, show the largest interannual (relative) SMB variability. Interestingly, these coincide with the EAP ice shelves, which are also sensitive to disintegration. The other SMB components (not shown) have low variability and show no pronounced patterns.

There are no trends in integrated precipitation, but Fig. 9a shows that large trends exist on a local scale, e.g. on Alexander Island and in the Weddell Sea these are significant. The model simulates large positive trends over the northerly slopes of the WAP (15 $\mathrm{mm\ w.e.\ y^{-2}}$), but these are not significant as these locations also inhibit large interannual variability. These trends are related to enhanced upper atmosphere northerly winds (Thomas et al., 2013; Van Wessem et al., 2015). Negative trends in snowmelt (Fig. 9b) are more significant on the WAP than on the EAP ice shelves, and show a uniform pattern.

4.3.2 Seasonal cycle

Figure 10 shows the average seasonal cycle (1979–2014) of SMB components. Integrated AP precipitation has a pronounced seasonality, with considerably larger values in winter than in summer. In winter, the stronger westerlies create more orographic precipitation over the WAP mountain slopes. In addition, WAP (and hence total) precipitation shows two peaks in March and in October, that are related to the semiannual cycle (van Loon, 1967; Van Den Broeke, 1998), in agreement with observational data from surface stations (Turner et al., 1997; Kirchgäß ner, 2011). Over the EAP, the precipitation seasonality is reversed: here precipitation peaks in summer reaching values almost as high as in the WAP summer, and decreases to a relatively constant minimum in winter an order of magnitude lower than over the WAP. Over the EAP, most summer precipitation originates from the Weddell Sea; when a minimum in sea-ice cover is reached in summer, moist ocean air is transported to the eastern ice shelves.

The other SMB components have lower magnitudes and show varying seasonal patterns. Snowmelt is absent in winter, reaches its peak (13 $\mathrm{Gt\ y^{-1}}$) in December and January. $\mathrm{SU_s}$ is negative in winter (–1 $\mathrm{Gt\ y^{-1}}$), when a persistent surface-based temperature inversion favours surface deposition. This positive contribution to the SMB is compensated by the stronger wintertime winds removing mass by $\mathrm{SU_{ds}}$. In summer, $\mathrm{SU_{ds}}$ drops off as winds are weaker and the snowpack gets warmer and denser. $\mathrm{SU_s}$ increases with surface temperature, and up to 3 $\mathrm{Gt\ y^{-1}}$ of snow is removed. Finally, $\mathrm{ER_{ds}}$ is very low year-round (<0.1 $\mathrm{Gt\ y^{-1}}$).

4.3.3 Spatial coherence of modelled precipitation

To illustrate the spatial coherence of AP SMB, Figure 11 shows the spatial correlation of the modelled yearly timeseries at the six ice core locations of Sect. 3.2, with all other points in the model domain. Figure 11a shows that the SMB at the Gomez ice core, in southwestern Palmer Land, is strongly and significantly (>99%) correlated over the whole WAP, acknowledging the strong spatial coherence that was also found for (observed) temperature in King (2003). Simultaneously there is a negative correlation over the northeastern AP, and Larsen B and C ice shelves, showing that high WAP SMB rates are coinciding with dry conditions over this region, a coherence not found in King (2003). Figure 11b identifies the spatial coherence of this location as well: when SMB is large at James Ross Island, it is large over the northern EAP ice shelves and sea-ice, while over the WAP an insignificant correlation is found. Figure 11c shows that the record at Dyer Plateau, which is located slightly east of the ice divide, is highly correlated with and representative of the adjacent EAP. Simultaneously, the second ice core at Dyer Plateau (Fig 11d), located only 30 km westwards, and the Bryan Coast and Ferrigno ice cores (Figs.11e,f), all located on the WAP, show completely opposite correlations, that closely resemble that of the Gomez ice core. These correlation maps clearly highlight the different forcing mechanisms of SMB on the WAP and EAP and the distinct and sharp climatic differences between both sides of the AP: over the WAP snowfall is orographically induced, while over the EAP it is brought in by depressions over the Weddell Sea.

5 Discussion

Although RACMO2.3 simulates the AP SMB with reasonable skill, the scarcity of observational data hampers a more thorough model assessment; more observational data should therefore be obtained, especially from higher elevations and areas with large snowfall rates. The comparison suggests that there are a number of potential problems. Not all local topographic detail (often at scales of < 1 km) is resolved at the 5.5 km model resolution. As a result the slope and the height of the orographic barrier of the AP are still underestimated, effecting uplift of air and, consequently, precipitation and atmospheric foehn winds. In previous research (Kuipers Munneke et al., 2012; Barrand et al., 2013; Trusel et al., 2013) it was suggested that increasing the horizontal resolution from 27 km to the current value of 5.5 km would better resolve EAP surface melt, that is strongly related to the foehn winds. While the increase in resolution is clearly an improvement for other topography related variables, it appears that these foehn winds are not yet sufficiently resolved. However, further increasing the resolution potentially moves the model beyond the limits of the hydrostatic assumption, and a non-hydrostatic model should then be used. Luckman et al. (2014) show that the non-hydrostatic, high-resolution (1.5 km) UTM model more efficiently resolves these foehn patterns. Cassano and Parish (2000) discussed the effects of a non-hydrostatic model on katabatic winds, which are also strongly related to the topography, and found that biases are relatively independent of the resolution.

Over the WAP there likely is a westward displacement of precipitation due to the model not taking into account horizontal advection of precipitation. In the current model version, precipitation is assumed to fall to the surface instantaneously within the grid box where it is generated. Ideally precipitation, in particular snow which has a relatively low fall speed, must be modelled as a prognostic variable in order to capture its fall time and horizontal displacement. Van Lipzig et al. (2004) estimated that, with mean wind speeds of $\sim$7 $\mathrm{m\,s^{-1}}$ for this region, snowfall could be advected over a distance of $\sim$10 km, ie.e roughly two grid boxes at 5.5 km resolution simulation.

Currently, the only prognostic cloud variables are water vapour and cloud water content, that, together with temperature, determine the fractionation of cloud ice and cloud liquid water. An explicit treatment of liquid and solid cloud content is more physical than the current implicit treatment using temperature. Improving this necessitates the inclusion of prognostic precipitation in future simulations, which potentially leads to more (and thicker) clouds to be advected over the mountain range, as well as an improvement of the biases in the downwelling radiative fluxes as found by King et al. (2015).

6 Summary and conclusions

We used the regional atmospheric climate model RACMO2.3 and a Firn Densification Model (FDM) to simulate the SMB of the Antarctic Peninsula at a horizontal resolution of 5.5 km. RACMO2.3 is forced by ERA-Interim reanalysis at the lateral boundaries, and the snowpack is initialized with output from the FDM. We have evaluated the simulated SMB by comparison with 132 in-situ SMB observations and 6 glacier discharge basins, both showing reasonable agreement. Most model biases are likely due to the still limited horizontal resolution, and limitations in the model physics e.g. the model being hydrostatic. However, the observations show a large over-representation from areas of low accumulation, especially over the western AP (WAP), and more observations are needed at higher elevations, regions of high accumulation and from the eastern AP (EAP), for a more robust model evaluation.

Integrated over four AP drainage basins (Zwally et al., 2012), the SMB amounts to 351 $\pm$ 58 Gt $\mathrm{y^{-1}}$ (σ = interannual variability), more or less equal to total precipitation (365 $\pm$ 57 Gt $\mathrm{y^{-1}}$), indicating that this is the major SMB component. The other components are more than an order of magnitude smaller, with drifting snow sublimation being the largest (9 $\pm$ 1.5 Gt $\mathrm{y^{-1}}$). Runoff is small (4 $\pm$ 4 Gt $\mathrm{y^{-1}}$) as most meltwater (34 $\pm$ 15 Gt $\mathrm{y^{-1}}$) and rainfall refreezes (33 $\pm$ 12 Gt $\mathrm{y^{-1}}$) in the cold firn, but is locally important on Larsen B, Larsen C and George VI ice shelves, and over the northwestern AP with values up to 200 $\mathrm{mm\ w.e.\ y^{-1}}$.

Pronounced differences in SMB exist between the WAP and EAP, and the AP spine acts as a sharp climate boundary. The SMB over the WAP amounts to 276 $\pm$ 47 Gt $\mathrm{y^{-1}}$, nearly a factor 4 larger than that over the EAP (75 $\pm$ 11 Gt $\mathrm{y^{-1}}$), resulting from the extreme orographic precipitation (>3000

$\mathrm{mm\ w.e.\ y^{-1}}$) the model simulates over the windward mountain slopes, especially in winter. Over the EAP, the seasonality in SMB is reversed, peaking in summer when sea-ice extent in the Weddell Sea is smallest and synoptic weather systems transport clouds to the AP from the east. The other SMB components do not show these large west-to-east differences, except for runoff. While melt rates are relatively similar over both the WAP and the EAP (18.7 ± 9,15.5 ± 6 Gt $\mathrm{y^{-1}}$), on the WAP most meltwater is retained or refreezes in the snowpack, that contains much pore space as a result of the large WAP snowfall rates. On the EAP snowmelt often exceeds precipitation, and not enough pore space is available for the meltwater to refreeze in, resulting in meltwater run off in the ocean (4 ± 4 Gt $\mathrm{y^{-1}}$). This makes total sublimation the largest ablation term in the integrated AP surface mass budget (11 ± 2 Gt $\mathrm{y^{-1}}$), which is primarily determined by drifting snow sublimation (9 ± 1 Gt $\mathrm{y^{-1}}$).

This new high-resolution AP dataset considerably adds to the current lower resolution data-sets such as ERA-Interim, or lower resolution simulations of RACMO2.3, as the mountainous terrain is much better resolved. These data can be used, in combination with satellite products such as GRACE and radar/laser altimetry, to better understand the changes of AP glaciers and ice shelves.

In order to further improve model results, a computationally more expensive non-hydrostatic model could be used for longer climate-scale simulations of specifically selected small and topographically complex areas of the AP. Moreover, the FDM can be updated to better represent meltwater percolation and refreezing, e.g. taking into account non-homogenous meltwater percolation. Additionally, more observational data of the AP, both remote sensing and in-situ data, should be acquired for model evaluation.

Acknowledgements. We are grateful for the financial support of NWO/ALW, Netherlands Polar Programme. We thank the ECMWF for the use of their supercomputing facilities. Graphics and calculations were made using the NCAR Command Language (Version 6.2.1, 2014).

References

Abram, N. J., Mulvaney, R., Wolff, E. W., Triest, J., Kipfstuhl, S., Trusel, L. D., Vimeux, F., Fleet, L., and Arrowsmith, C.: Acceleration of snow melt in an Antarctic Peninsula ice core during the twentieth century, Nature Geoscience, 6, 404–411, doi:10.1038/ngeo1787, http://www.nature.com/doifinder/10.1038/ngeo1787, 2013.

Aristarain, A. J., Delmas, R. J., and Stievenard, M.: ICE-CORE STUDY OF THE LINK BETWEEN SEA-SALT AEROSOL, SEA-ICE COVER AND CLIMATE IN THE ANTARCTIC PENINSULA AREA, Climatic Change, 67, 63–86, 2004.

Arthern, R. J., Vaughan, D. G., Rankin, A. M., Mulvaney, R., and Thomas, E. R.: In situ measurements of Antarctic snow compaction compared with predictions of models, Journal of Geophysical Research, 115, F03 011, doi:10.1029/2009JF001306, http://doi.wiley.com/10.1029/2009JF001306, 2010.

Bamber, J. and Gomez-Dans, J.: A new 1 km digital elevation model of the Antarctic derived from combined satellite radar and laser data Part 1 : Data and methods, The Cryosphere, 3, 101–111, http://content.imamu.edu.sa/Scholars/it/net/tc-3-101-2009.pdf, 2009.

Barrand, N. E., Vaughan, D. G., Steiner, N., Tedesco, M., Kuipers Munneke, P., van den Broeke, M. R., and Hosking, J. S.: Trends in Antarctic Peninsula surface melting conditions from observations and regional climate modeling, Journal of Geophysical Research: Earth Surface, 118, 315–330, doi:10.1029/2012JF002559, http://doi.wiley.com/10.1029/2012JF002559, 2013.

Bromwich, D. H.: Modeled Antarctic Precipitation. Part I: Spatial and Temporal Variability, Journal of Climate, pp. 427–448, 2004.

Bromwich, D. H., Nicolas, J. P., Hines, K. M., Kay, J. E., Key, E. L., Lazzara, M. A., Lubin, D., Mcfarquhar, G. M., Gorodetskaya, I. V., Grosvenor, D. P., Cope, T. L., and Lipzig, N. P. M. V.: Tropospheric Clouds in Antarctica, Reviews of Geophysics, 50, 1–40, doi:10.1029/2011RG000363.1.INTRODUCTION, 2012.

Cassano, J. J. and Parish, T. R.: An Analysis of the Nonhydrostatic Dynamics in Numerically Simulated Antarctic Katabatic Flows*, Journal of the Atmospheric Sciences, 57, 891–898, doi:10.1175/1520-0469(2000)057⟨0891:AAOTND⟩2.0.CO;2, http://journals.ametsoc.org/doi/abs/10.1175/1520-0469\%282000\%29057\%3C0891\%3AAAOTND\%3E2.0.CO\%3B2, 2000.

Cook, A. J., Fox, A. J., Vaughan, D. G., and Ferrigno, J. G.: Retreating glacier fronts on the Antarctic Peninsula over the past half-century., Science (New York, N.Y.), 308, 541–4, doi:10.1126/science.1104235, http://www.ncbi.nlm.nih.gov/pubmed/15845851, 2005.

Cook, A. J., Murray, T., Luckman, A., Vaughan, D. G., and Barrand, N. E.: A new 100-m Digital Elevation Model of the Antarctic Peninsula derived from ASTER Global DEM: methods and accuracy assessment, Earth System Science Data, 4, 129–142, doi:10.5194/essd-4-129-2012, http://www.earth-syst-sci-data.net/4/129/2012/, 2012.

Davis, C. H., Li, Y., McConnell, J. R., Frey, M. M., and Hanna, E.: Snowfall-driven growth in East Antarctic ice sheet mitigates recent sea-level rise., Science (New York, N.Y.), 308, 1898–1901, doi:10.1126/science.1110662, 2005.

Dee, D. P., Uppala, S. M., Simmons, A. J., Berrisford, P., Poli, P., Kobayashi, S., Andrae, U., Balmaseda, M. A., Balsamo, G., Bauer, P., Bechtold, P., Beljaars, A. C. M., Van de Berg, L., Bidlot, J., Bormann, N., Delsol, C., Dragani, R., Fuentes, M., Geer, A. J., Haimberger, L., Healy, S. B., Hersbach, H., Hólm,

E. V., Isaksen, L., Kå llberg, P., Köhler, M., Matricardi, M., McNally, A. P., Monge-Sanz, B. M., Morcrette, J. J., Park, B. K., Peubey, C., de Rosnay, P., Tavolato, C., Thépaut, J. N., and Vitart, F.: The ERA-Interim reanalysis: configuration and performance of the data assimilation system, Quarterly Journal of the Royal Meteorological Society, 137, 553–597, doi:10.1002/qj.828, http://doi.wiley.com/10.1002/qj.828, 2011.

Dupont, T. K. and Alley, R. B.: Assessment of the importance of ice-shelf buttressing to ice-sheet flow, Geophysical Research Letters, 32, 1–4, doi:10.1029/2004GL022024, 2005.

Ettema, J., Van den Broeke, M. R., Van Meijgaard, E., Van de Berg, W. J., Box, J. E., and Steffen, K.: Climate of the Greenland ice sheet using a high-resolution climate model Part 1: Evaluation, The Cryosphere, 4, 511–527, doi:10.5194/tc-4-511-2010, http://www.the-cryosphere.net/4/511/2010/, 2010.

Favier, V., Agosta, C., Parouty, S., Durand, G., Delaygue, G., Gallée, H., Drouet, A.-S., Trouvilliez, A., and Krinner, G.: An updated and quality controlled surface mass balance dataset for Antarctica, The Cryosphere, 7, 583–597, doi:10.5194/tc-7-583-2013, http://www.the-cryosphere.net/7/583/2013/, 2013.

Fettweis, X.: The Cryosphere Reconstruction of the 1979 - 2006 Greenland ice sheet surface mass balance using the regional climate model MAR, The Cryosphere, 1, 21–40, 2007.

Gunter, B., Urban, T., Riva, R., Helsen, M., Harpold, R., Poole, S., Nagel, P., Schutz, B., and Tapley, B.: A comparison of coincident GRACE and ICESat data over Antarctica, Journal of Geodesy, 83, 1051–1060, doi:10.1007/s00190-009-0323-4, http://link.springer.com/10.1007/s00190-009-0323-4, 2009.

King, J. C.: The spatial coherence of interannual temperature variations in the Antarctic Peninsula, Geophysical Research Letters, 30, 1040, doi:10.1029/2002GL015580, http://doi.wiley.com/10.1029/2002GL015580, 2003.

King, J. C., Gadian, A., Kirchgaessner, A., Munneke, P. K., Orr, A., Reijmer, C., Broeke, M. R., Van Wessem, J. M., and Weeks, M.: Validation of the summertime surface energy budgetof Larsen C Ice Shelf (Antarctica) as representedin three high-resolution atmospheric models, Journal of Geophysical Research: Atmospheres, pp. 1–13, doi:10.1002/2014JD022604.Received, 2015.

Kirchgäß ner, A.: An analysis of precipitation data from the Antarctic base Faraday/Vernadsky, International Journal of Climatology, 31, 404–414, doi:10.1002/joc.2083, http://doi.wiley.com/10.1002/joc.2083, 2011.

Kuipers Munneke, P., Van den Broeke, M. R., Lenaerts, J. T. M., Flanner, M. G., Gardner, A. S., and Van de Berg, W. J.: A new albedo parameterization for use in climate models over the Antarctic ice sheet, Journal of Geophysical Research, 116, 1–10, doi:10.1029/2010JD015113, http://www.agu.org/pubs/crossref/2011/2010JD015113.shtml, 2011.

Kuipers Munneke, P., Picard, G., van den Broeke, M. R., Lenaerts, J. T. M., and van Meijgaard, E.: Insignificant change in Antarctic snowmelt volume since 1979, Geophysical Research Letters, 39, 6–10, doi:10.1029/2011GL050207, http://www.agu.org/pubs/crossref/2012/2011GL050207.shtml, 2012.

Kuipers Munneke, P., Ligtenberg, S. R. M., Van Den Broeke, M. R., and Vaughan, D. G.: Firn air depletion as a precursor of Antarctic ice-shelf collapse, Journal of Glaciology, 60, 205–214, doi:10.3189/2014JoG13J183, http://www.igsoc.org/journal/60/220/t13J183.html, 2014.

Kuipers Munneke, P., Ligtenberg, S. R., Suder, E. a., and Van Den Broeke, M. R.: A model study of the response of dry and wet firn to climate change, Annals of Glaciology, 56, 1–8, doi:10.3189/2015AoG70A994, http://www.igsoc.org/annals/56/70/t70a994.html, 2015.

Lenaerts, J. T. M., Van den Broeke, M. R., Déry, S. J., Van Meijgaard, E., Van de Berg, W. J., Palm, S. P., and

Sanz Rodrigo, J.: Modeling drifting snow in Antarctica with a regional climate model: 1. Methods and model evaluation, Journal of Geophysical Research, 117, 1–17, doi:10.1029/2011JD016145, http://www.agu.org/pubs/crossref/2012/2011JD016145.shtml, 2012a.

Lenaerts, J. T. M., Van den Broeke, M. R., Van de Berg, W. J., Van Meijgaard, E., and Kuipers Munneke, P.: A new, high-resolution surface mass balance map of Antarctica (1979-2010) based on regional atmospheric climate modeling, Geophysical Research Letters, 39, 1–5, doi:10.1029/2011GL050713, http://www.agu.org/pubs/crossref/2012/2011GL050713.shtml, 2012b.

Lenaerts, J. T. M., Van den Broeke, M. R., Van Wessem, J. M., Van de Berg, W. J., Van Meijgaard, E., Van Ulft, L. H., and Schaefer, M.: Extreme precipitation and climate gradients in Patagonia revealed by high-resolution regional atmospheric climate modelling, Journal of Climate, p. 140404144919009, doi:10.1175/JCLI-D-13-00579.1, http://journals.ametsoc.org/doi/abs/10.1175/JCLI-D-13-00579.1, 2014.

Ligtenberg, S. R. M., Helsen, M. M., and van den Broeke, M. R.: An improved semi-empirical model for the densification of Antarctic firn, The Cryosphere, 5, 809–819, doi:10.5194/tc-5-809-2011, http://www.the-cryosphere.net/5/809/2011/, 2011.

Ligtenberg, S. R. M., Kuipers Munneke, P., and van den Broeke, M. R.: Present and future variations in Antarctic firn air content, The Cryosphere, 8, 1711–1723, doi:10.5194/tc-8-1711-2014, http://www.the-cryosphere.net/8/1711/2014/, 2014.

Luckman, A., Elvidge, A., Jansen, D., Kulessa, B., Kuipers Munneke, P., King, J., and Barrand, N. E.: Surface melt and ponding on Larsen C Ice Shelf and the impact of föhn winds, Antarctic Science, 26, 625–635, doi:10.1017/S0954102014000339, http://www.journals.cambridge.org/abstract_S0954102014000339, 2014.

Mouginot, J., Scheuchl, B., and Rignot, E.: Mapping of Ice Motion in Antarctica Using Synthetic-Aperture Radar Data, Remote Sensing, 4, 2753–2767, doi:10.3390/rs4092753, http://www.mdpi.com/2072-4292/4/9/2753/, 2012.

Peel, D. A.: Ice core evidence from the Antarctic Peninsula region, Climate since AD, 1500, 549–571, 1992.

Pritchard, H. D., Ligtenberg, S. R. M., Fricker, H. A., Vaughan, D. G., Van den Broeke, M. R., and Padman, L.: Antarctic ice-sheet loss driven by basal melting of ice shelves., Nature, 484, 502–5, doi:10.1038/nature10968, http://www.ncbi.nlm.nih.gov/pubmed/22538614, 2012.

Rignot, E., Velicogna, I., Van den Broeke, M. R., Monaghan, A., and Lenaerts, J. T. M.: Acceleration of the contribution of the Greenland and Antarctic ice sheets to sea level rise, Geophysical Research Letters, 38, 1–5, doi:10.1029/2011GL046583, http://www.agu.org/pubs/crossref/2011/2011GL046583.shtml, 2011.

Scambos, T. A., Hulbe, C., Fahnestock, M., and Bohlander, J.: The link between climate warming and break-up of ice shelves in the Antarctic Peninsula, Journal of Glaciology, 46, 516–530, doi:10.3189/172756500781833043, http://openurl.ingenta.com/content/xref?genre=article\&issn=0022-1430\&volume=46\&issue=154\&spage=516, 2000.

Scambos, T. A., Berthier, E., Haran, T., Shuman, C. A., Cook, A. J., Ligtenberg, S. R. M., and Bohlander, J.: Detailed ice loss pattern in the northern Antarctic Peninsula: widespread decline driven by ice front retreats, The Cryosphere, 8, 2135–2145, doi:10.5194/tc-8-2135-2014, http://www.the-cryosphere.net/8/2135/2014/, 2014.

Shepherd, A., Ivins, E. R., A, G., Barletta, V. R., Bentley, M. J., Bettadpur, S., Briggs, K. H., Bromwich, D. H., Forsberg, R., Galin, N., Horwath, M., Jacobs, S., Joughin, I., King, M. A., Lenaerts, J. T. M., Li,

J., Ligtenberg, S. R. M., Luckman, A., Luthcke, S. B., McMillan, M., Meister, R., Milne, G., Mouginot, J., Muir, A., Nicolas, J. P., Paden, J., Payne, A. J., Pritchard, H., Rignot, E., Rott, H., Sorensen, L. S., Scambos, T. A., Scheuchl, B., Schrama, E. J. O., Smith, B., Sundal, A. V., Van Angelen, J. H., Van de Berg, W. J., Van den Broeke, M. R., Vaughan, D. G., Velicogna, I., Wahr, J., Whitehouse, P. L., Wingham, D. J., Yi, D., Young, D., and Zwally, H. J.: A Reconciled Estimate of Ice-Sheet Mass Balance, Science, 338, 1183–1189, doi:10.1126/science.1228102, http://www.sciencemag.org/cgi/doi/10.1126/science.1228102, 2012.

Tapley, B. D., Bettadpur, S., and Watkins, M.: The Gravity Recovery and Climate Experiment: Mission Overview and Early Results, Geophysical Research Letters, 31, 2004.

Thomas, E. R., Marshall, G. J., and McConnell, J. R.: A doubling in snow accumulation in the western Antarctic Peninsula since 1850, Geophysical Research Letters, 35, 1–5, doi:10.1029/2007GL032529, http://www.agu.org/pubs/crossref/2008/2007GL032529.shtml, 2008.

Thomas, E. R., Bracegirdle, T. J., Turner, J., and Wolff, E. W.: A 308 year record of climate variability in West Antarctica, Geophysical Research Letters, 40, n/a–n/a, doi:10.1002/2013GL057782, http://doi.wiley.com/10.1002/2013GL057782, 2013.

Thompson, L., Peel, D., Mosley-Thompson, E., Mulvaney, R., Dal, J., Lin, P., Davis, M., and Raymond, C.: Climate since AD 1510 on Dyer Plateau, Antarctic Peninsula: evidence for recent climate change, Annals of Glaciology, 20, 420–426, doi:10.3189/172756494794587438, http://www.ingentaconnect.com/content/igsoc/agl/1994/00000020/00000001/art00067, 1994.

Trusel, L. D., Frey, K. E., Das, S. B., Kuipers Munneke, P., and van den Broeke, M. R.: Satellite-based estimates of Antarctic surface meltwater fluxes, Geophysical Research Letters, 40, n/a–n/a, doi:10.1002/2013GL058138, http://doi.wiley.com/10.1002/2013GL058138, 2013.

Turner, J., Colwell, S. R., and Harangozo, S.: Variability of precipitation over the coastal western Antarctic Peninsula from synoptic observations, Journal of Geophysical Research, 102, 13 999, doi:10.1029/96JD03359, 1997.

Turner, J., Marshall, G. J., Morris, E. M., Mulvaney, R., and Winter, W.: Spatial variability of Antarctic Peninsula net surface mass balance, Journal of Geophysical Research, 107, 2002.

Turner, J., Colwell, S. R., Marshall, G. J., Lachlan-Cope, T. A., Carleton, A. M., Jones, P. D., Lagun, V., Reid, P. A., and Iagovkina, S.: Antarctic climate change during the last 50 years, International Journal of Climatology, 25, 279–294, doi:10.1002/joc.1130, http://dx.doi.org/10.1002/joc.1130, 2005.

UCAR/NCAR/CISL/VETS: The NCAR Command Language (Version 6.2.1) [Software]. (2014), doi:http://dx.doi.org/10.5065/D6WD3XH5, 2014.

Undén, P., Rontu, L., Jarvinen, H., Lynch, P., Calvo, J., Cats, G., Cuxart, J., Eerola, K., Fortelius, C., Garciamoya, J., Jones, C., Lenderlink, G., Mcdonald, A., Mcgrath, R., and Navascues, B.: HIRLAM-5 Scientific Documentation, Tech. Rep. December, Swedish Meteorology and Hydrology Institute, 2002.

Van Angelen, J. H., Van den Broeke, M. R., Wouters, B., and Lenaerts, J. T. M.: Contemporary (19602012) Evolution of the Climate and Surface Mass Balance of the Greenland Ice Sheet, Surveys in Geophysics, 35, 1155–1174, doi:10.1007/s10712-013-9261-z, http://link.springer.com/10.1007/s10712-013-9261-z, 2013.

Van Den Broeke, M. R.: The semi-annual oscillation and Antarctic climate. Part 2: recent changes, Antarctic Science, 10, 175–183, doi:10.1017/S095410209800025X, 1998.

Van den Broeke, M. R.: Strong surface melting preceded collapse of Antarctic Peninsula ice shelf, Geo-

physical Research Letters, 32, 2–5, doi:10.1029/2005GL023247, http://www.agu.org/pubs/crossref/2005/2005GL023247.shtml, 2005.

Van Lipzig, N. P. M., King, J. C., and Lachlan-Cope, T. A.: Precipitation, sublimation, and snow drift in the Antarctic Peninsula region from a regional atmospheric model, Journal of Geophysical Research, 109, 1–16, doi:10.1029/2004JD004701, http://www.agu.org/pubs/crossref/2004/2004JD004701.shtml, 2004.

van Loon, H.: The Half-Yearly Oscillations in Middle and High Southern Latitudes and the Coreless Winter, Journal of the Atmospheric Sciences, 24, 472–486, doi:10.1175/1520-0469(1967)024⟨0472:THYOIM⟩2.0.CO;2, 1967.

Van Wessem, J. M., Reijmer, C. H., Lenaerts, J. T. M., Van de Berg, W. J., Van den Broeke, M. R., and Van Meijgaard, E.: Updated cloud physics in a regional atmospheric climate model improves the modelled surface energy balance of Antarctica, The Cryosphere, 8, 125–135, doi:10.5194/tc-8-125-2014, http://www.the-cryosphere.net/8/125/2014/, 2014a.

Van Wessem, J. M., Reijmer, C. H., Morlighem, M., Mouginot, J., Rignot, E., Medley, B., Joughin, I., Wouters, B., Depoorter, M. A., Bamber, J. L., Lenaerts, J. T. M., Van De Berg, W. J., Van Den Broeke, M. R., and Van Meijgaard, E.: Improved representation of East Antarctic surface mass balance in a regional atmospheric climate model, Journal of Glaciology, 60, 761–770, doi:10.3189/2014JoG14J051, http://www.igsoc.org/journal/60/222/t14j051.html, 2014b.

Van Wessem, J. M., Reijmer, C. H., van de Berg, W. J., Cook, A. J., van den Broeke, M. R., Van Ulft, L. H., and van Meijgaard, E.: Temperature and wind climate of the Antarctic Peninsula as simulated by a high-resolution regional atmospheric climate model, Journal of Climate, 2015.

Vaughan, D. G., Marshall, G., Connolley, W. M., Parkinson, C., Mulvaney, R., Hodgson, D. A., King, J. C., Pudsey, C. J., and Turner, J.: Recent Rapid Regional Climate Warming on the Antarctic Peninsula, Climatic Change, 60, 243–274, 2003.

Wouters, B., Martin-Español, A., Helm, V., Flament, T., van Wessem, J. M., Ligtenberg, S. R. M., van den Broeke, M. R., and Bamber, J. L.: Glacier mass loss. Dynamic thinning of glaciers on the Southern Antarctic Peninsula., Science (New York, N.Y.), 348, 899–903, doi:10.1126/science.aaa5727, http://www.sciencemag.org/content/348/6237/899.abstract, 2015.

Wuite, J., Rott, H., Hetzenecker, M., Floricioiu, D., De Rydt, J., Gudmundsson, G. H., Nagler, T., and Kern, M.: Evolution of surface velocities and ice discharge of Larsen B outlet glaciers from 1995 to 2013, The Cryosphere, 9, 957–969, doi:10.5194/tc-9-957-2015, http://www.the-cryosphere.net/9/957/2015/tc-9-957-2015.html, 2015.

Zwally, H. J., Giovinetto, M. B., Beckley, M. A., and Saba, J. L.: Antarctic and Greenland Drainage Systems, http://icesat4.gsfc.nasa.gov/cryo_data/ant_grn_drainage_systems.php, 2012.

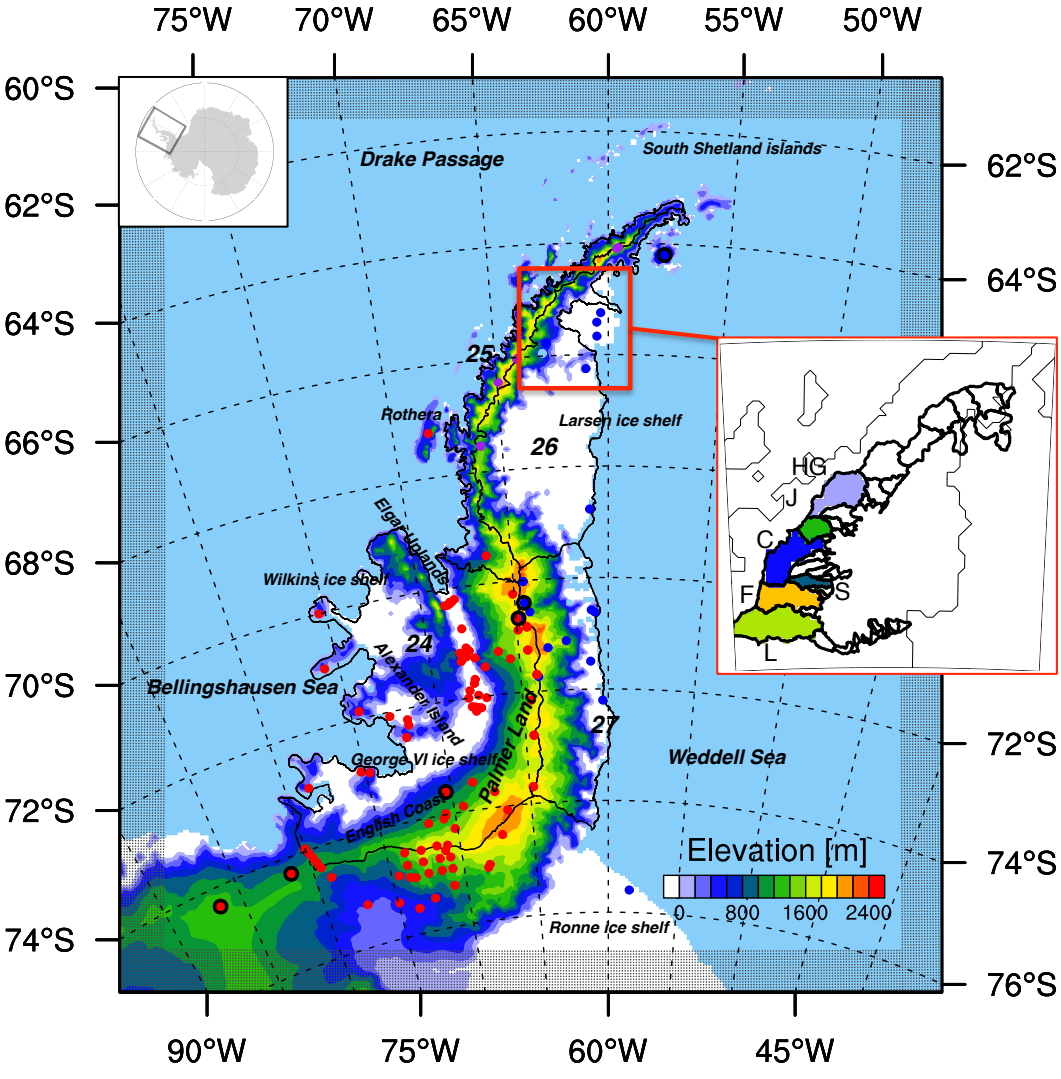

Fig. 1. RACMO2.3 Antarctic Peninsula model domain (black box in inset map of Antarctica), boundary relaxation zone (dotted area, 16 grid points) and model surface topography [m] of the Antarctic Peninsula. Locations of in-situ SMB observations are marked (dots); ice cores with a yearly accumulation record, as used in Sect. 3.2, are highlighted with a black circle. Colors of the dots represent whether the observation lies in a WAP (red), EAP (blue) or spine (purple) height bin (see Sect. 3 for more details). Model topography is based on digital elevation models from Cook et al. (2012) for the region north of 70° S. and Bamber and Gomez-Dans (2009) south of 70 ° S. White areas represent floating ice shelves, colours represent the elevation of the grounded ice sheet. Zwally et al. (2012) drainage basins 24, 25, 26 and 27 are shown (black contours). One EAP in-situ observation is shown in light blue for visibility. Inset denotes the 6 drainage basins of pre-acceleration Larsen B outlet glaciers: Starbuck (S), Flask (F), Leppard (L), Crane (C), Jorum (J) and Hektoria-Green (HG) from Wuite et al. (2015). T

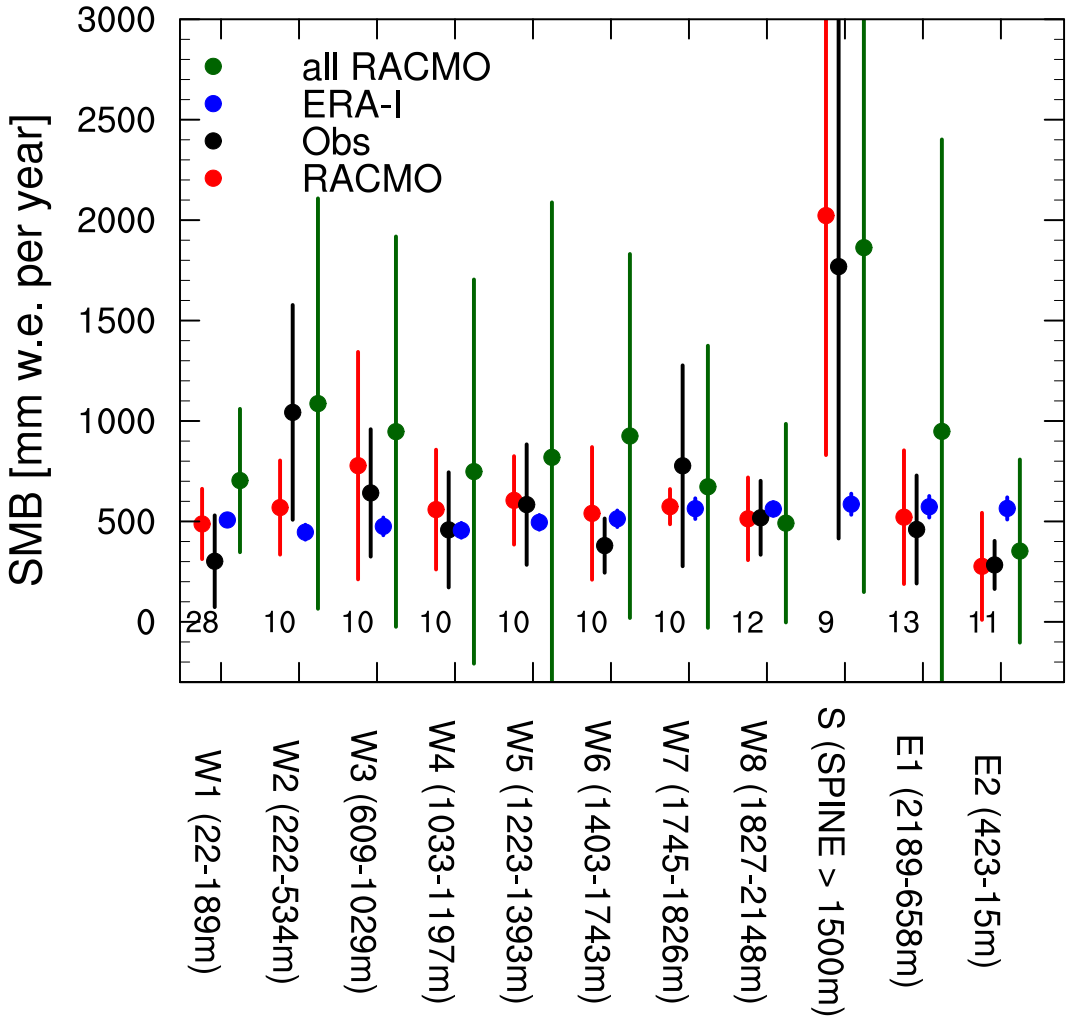

Fig. 2. Modelled (red), ERA-Interim (blue) and observed (black) SMB as a function of eleven elevation bins for all in-situ SMB observations. The bins are chosen such that they include at least 10 data points and/or include a range of elevations of at least ∼75 m. The bins are arranged from west to east in three seperate classes (WAP (W1–8), the spine (S) and the EAP (E1–2)), using the drainage basin definition from Zwally et al. (2012): basins 24 or 25 represent W; basin 26 or 27 represent E; all points in either basin 26 or 27 and >1500 m elevation are included in S. For all other observations not located in either of the basins, but are within the model domain, we define a 65° W boundary: all observations west of this boundary represent W, the others E. The green dots are the average SMB of all RACMO points in the respective bins. Error bars represent one standard deviation within the bin and amount of observations in each bin is denoted within the plot. Further details are provided in Sect. 2.3.1.

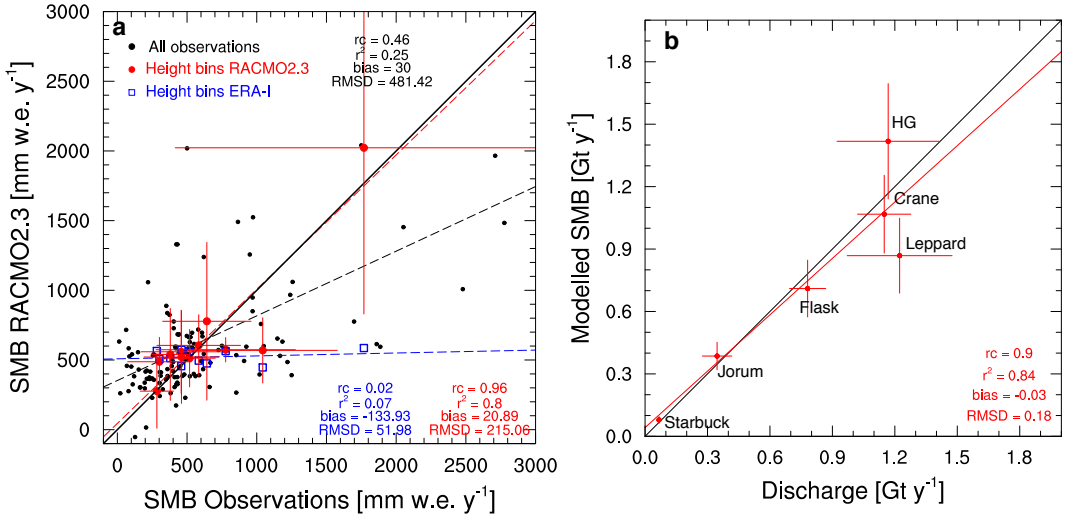

Fig. 3. a) Modelled SMB as a function of in-situ SMB observations (black dots), and the height bins as defined in Fig. 2) for RAMCO2.3 (red dots) and ERA-Interim (blue squares) in $\mathrm{mm\ w.e.\ y^{-1}}$. Error bars represent one standard deviation within the height bins. Dashed lines represent the linear regressions lines. Two in-situ observations with SMB values >3000 $\mathrm{mm\ w.e.\ y^{-1}}$ are off the chart and are not shown. b) Modelled SMB (with one standard deviation) as a function of drainage basins discharge estimates (with uncertainty) (Wuite et al., 2015) in $\mathrm{Gt\ y^{-1}}$. Red line represents the regression line of modelled SMB with discharge estimates.

Table 1. AP integrated values of mean SMB components [$\mathrm{Gt\ y^{-1}}$] with interannual variability σ: total (snow+rain) precipitation (PR), snow, rain, total sublimation ($\mathrm{SU_{tot}}$), surface sublimation ($\mathrm{SU_s}$), drifting snow sublimation ($\mathrm{SU_{ds}}$), drifting snow erosion ($\mathrm{ER_{ds}}$), runoff (RU), snowmelt (M) and refreezing (RF). All values are calculated for basins 24–27 of Zwally et al. (2012), over a total AP area of $4.1{\cdot}10^5\mathrm{km}^2$. For WAP and EAP values, basins 24/25 and 26/27 are used, respectively. Values are calculated from yearly averages; from 2003 onwards integrated values represent the ice shelf excluding Larsen B ice shelf.

	mean	σ	EAP	σ	WAP	σ
Area (km^2)	$4.1{\cdot}10^5$	–	$2.4{\cdot}10^5$	–	$1.7{\cdot}10^5$	
SMB	351	58	75	11	276	47
PR	365	57	84	10	281	47
snow	363	56	85	10	279	46
rain	3	1	0.5	0	2.2	1
SU	11	2	5.6	1	5.1	1
$\mathrm{SU_{ds}}$	9	2	4.1	1	5	1
$\mathrm{SU_s}$	2	0	1.6	0	0.1	0
$\mathrm{ER_{ds}}$	1	0	-0.6	0	1.4	0
M	34	15	18.7	9	15.5	6
RF	35	13	17.2	6	17.5	7
RU	4	4	3.8	4	0.2	0

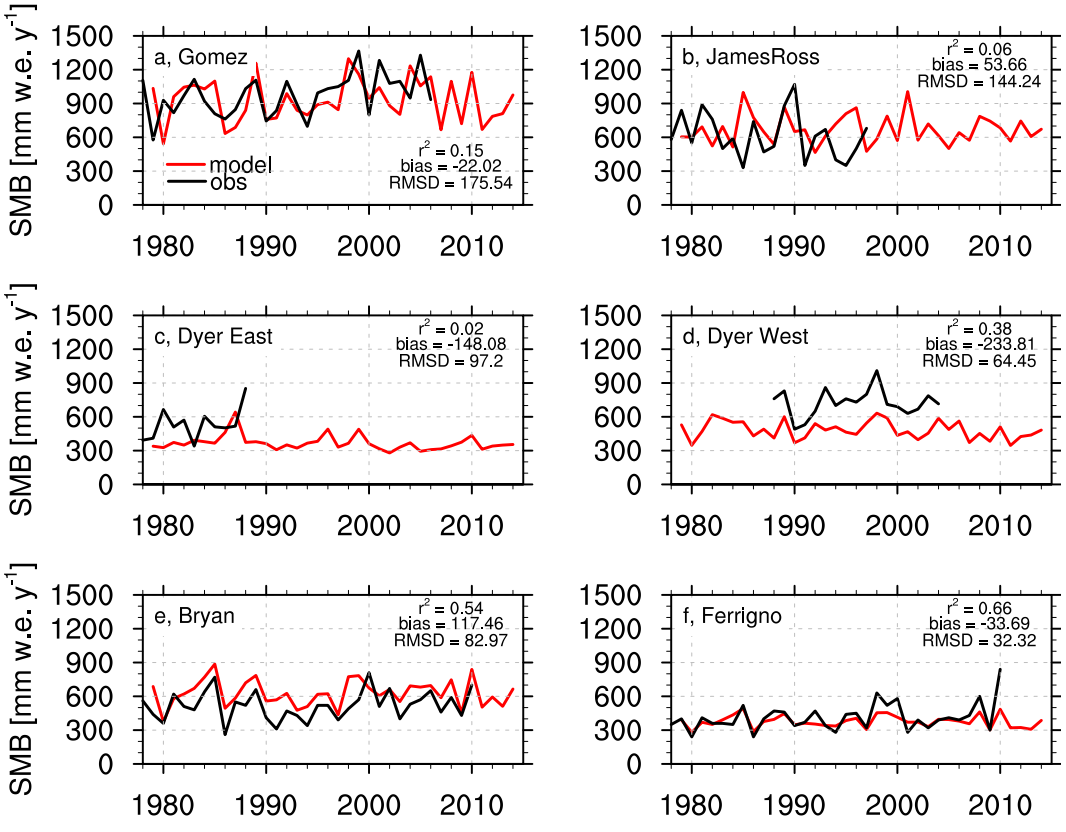

Fig. 4. Modelled and observed yearly (1979–2014) SMB ($\mathrm{mm\ w.e.\ y^{-1}}$) at locations of Gomez (a, 73°S, 70°W), James Ross Island (b, 64.2°S, 57.7°W), Dyer Plateau East (c, 70.4°S, 64.5°W), Dyer Plateau West (d, 70.7°S, 64.9°W), Bryan Coast (e, 74.3°S, 81.4°W) and Ferrigno (f, 74.3°S, 86.5°W) ice cores. Statistics (r^2, bias and RMSD) are denoted.

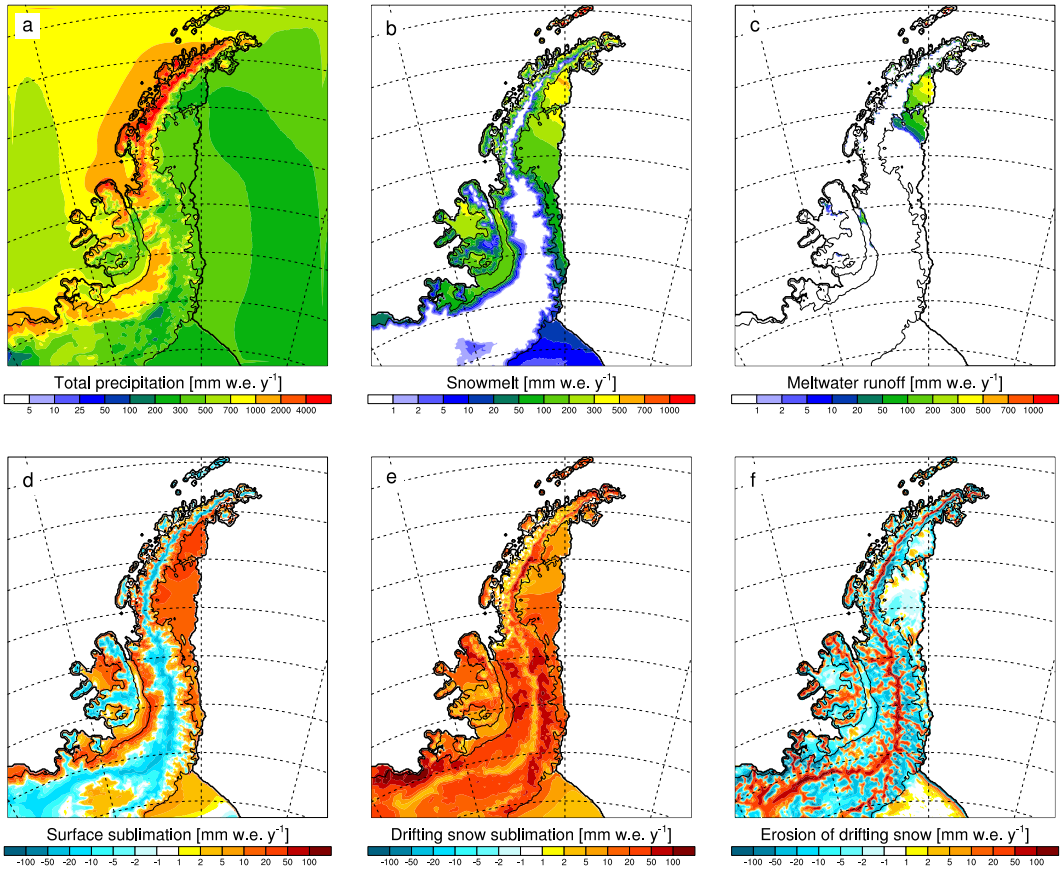

Fig. 5. 1979–2014 average SMB components: Total precipitation (snowfall + rain) (a), snowmelt (b), meltwater runoff (c), total sublimation (d), sublimation of drifting snow (e) and erosion of drifting snow (f) in $\mathrm{mm\ w.e.\ y^{-1}}$. Note that ablation is defined positive in Figs. d,e,f. All fluxes are from RACMO2.3, except for runoff, which is calculated by the FDM that is forced by RACMO2.3 output.

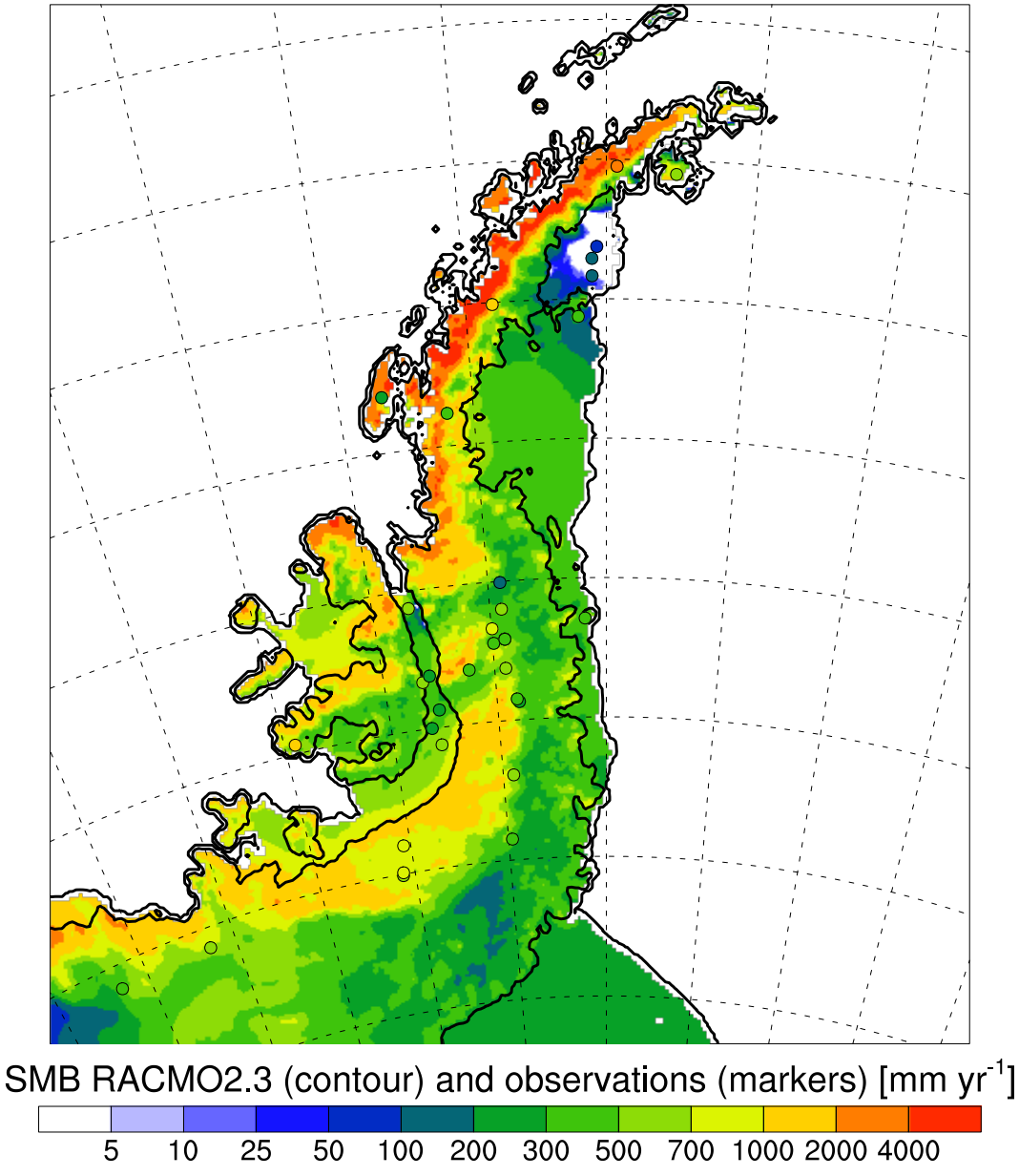

Fig. 6. Modelled SMB (colours) and observations (markers) in $\mathrm{mm\ w.e.\ y^{-1}}$. Observations are from Turner et al. (2002); Favier et al. (2013); Scambos et al. (2014) and sources noted in Sect. 2.3, and only shown if they represent a period >5 years. Modelled SMB is the 1979–2014 climatological average.

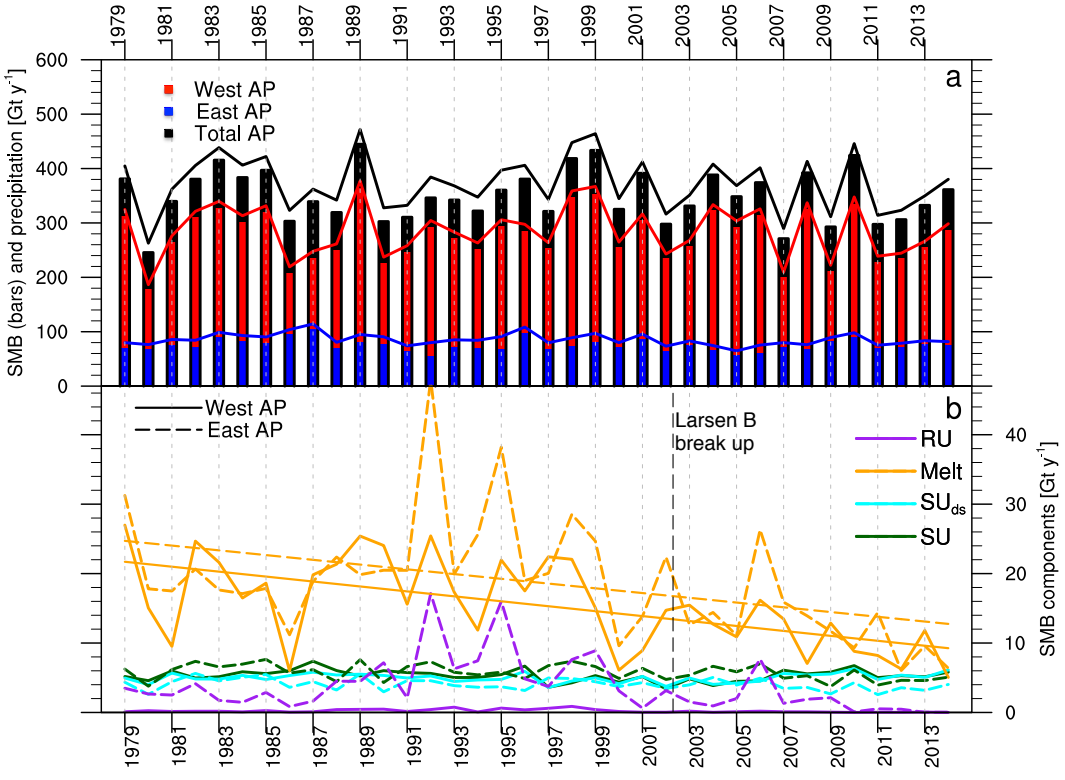

Fig. 7. Yearly average SMB components in $\mathrm{Gt\ y^{-1}}$. For SMB, values for the west AP (red) and the east (blue) are shown. SMB is integrated over basins 24, 25, 26 and 27 from Zwally et al. (2012). Trend lines are only shown if significant. From 2003 onwards integrated values represent the ice shelf excluding Larsen B ice shelf.

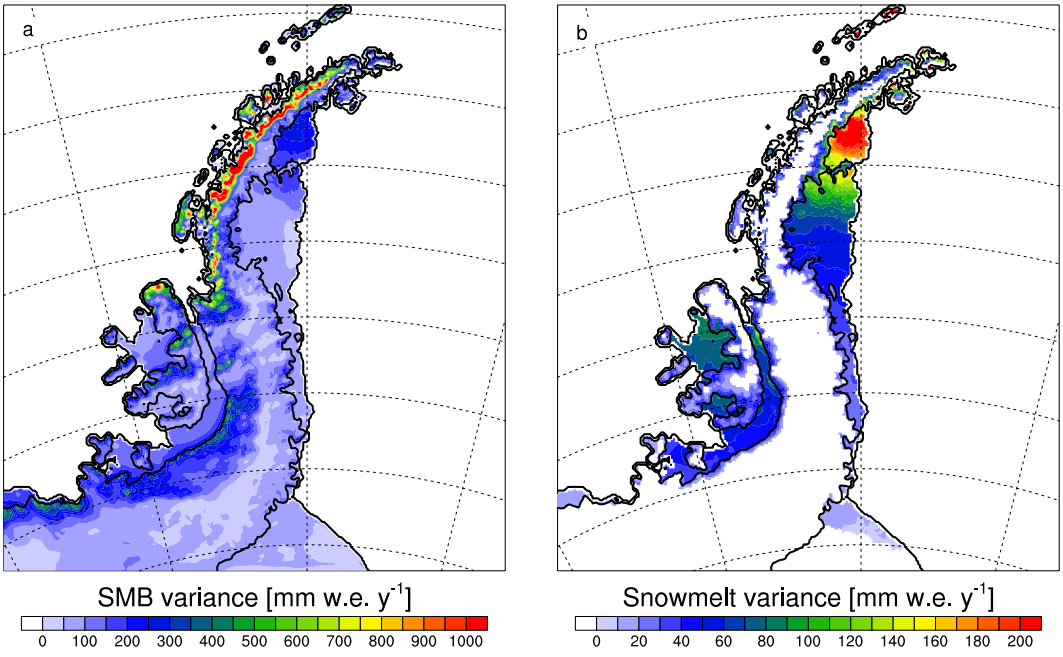

Fig. 8. Interannual variability (one standard deviation, detrended) of SMB components for 1979–2014: SMB (a), and snowmelt (b), in $\mathrm{mm\ w.e.\ y^{-1}}$.

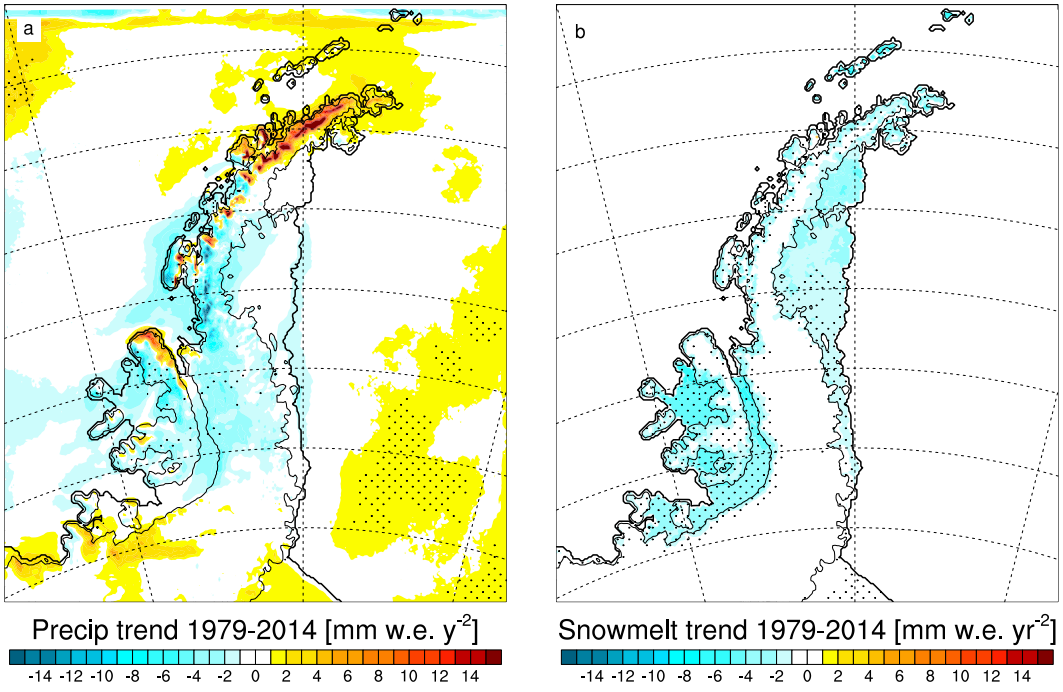

Fig. 9. 1979–2014 trends of snowmelt (a) and precipitation (b) in $\mathrm{mm\ w.e.\ y^{-2}}$. Stippled pattern represents trends that are significant >95%

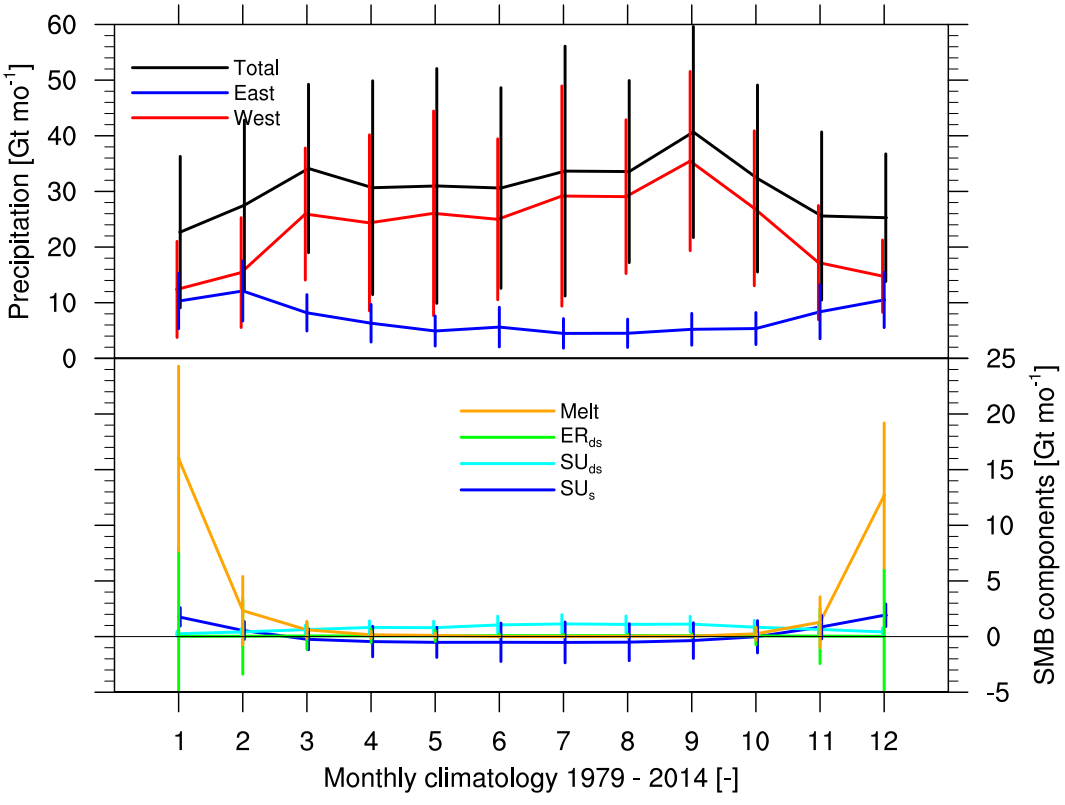

Fig. 10. 1979–2014 monthly climatology of SMB components: Top panel shows total precipitation (snowfall + rain) averaged for the WAP drainage basins (red line), the EAP (blue), and total (black). Bottom panel shows total (WAP+EAP) snowmelt (orange), erosion of drifting snow $\mathrm{ER_{ds}}$ (green), drifting snow sublimation $\mathrm{SU_{ds}}$ (cyan), and surface sublimation/deposition (blue). All variables in units $\mathrm{Gt\ y^{-1}}$.

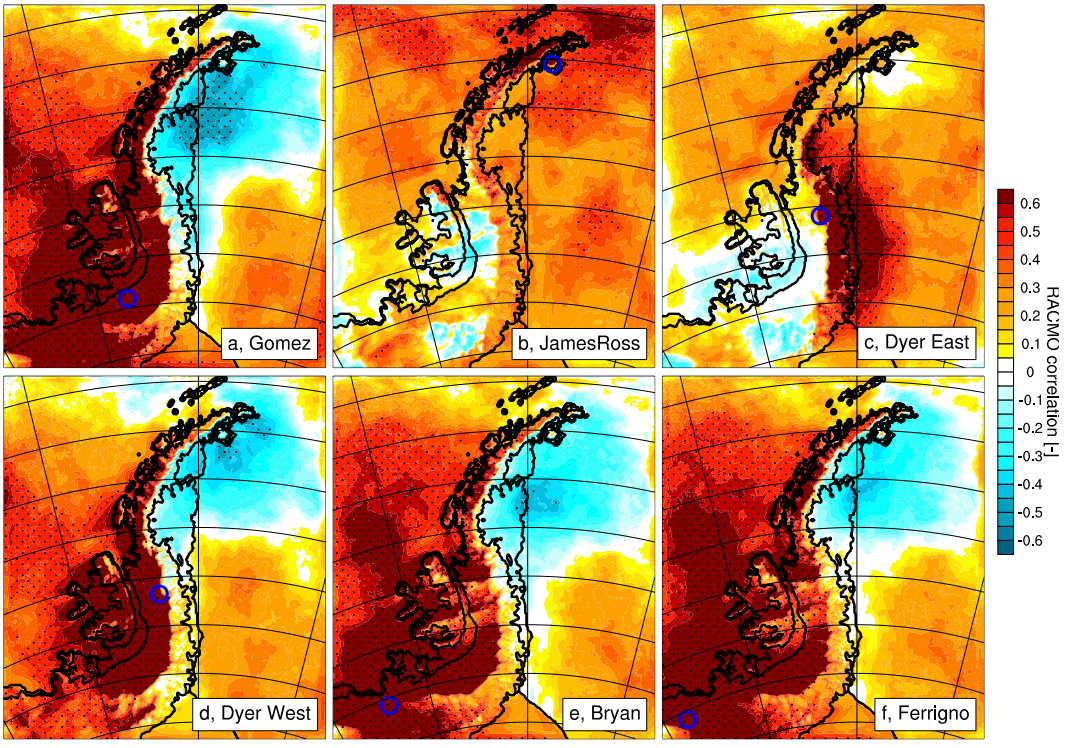

Fig. 11. Correlation of modelled yearly (1979–2014) SMB at locations of Gomez (a, 73°S, 70°W), James Ross Island (b, 64.2°S, 57.7°W), Dyer Plateau East (c, 70.4°S, 64.5°W), Dyer Plateau West (d, 70.7°S, 64.9°W), Bryan Coast (e, 74.3°S, 81.4°W) and Ferrigno (f, 74.3°S, 86.5°W) ice cores, with all other points in the model domain. Stippled pattern represents significant correlations >99%. Locations of ice cores are denoted by blue circles. Note that over the sea-ice/ocean $\mathrm{SMB} = \mathrm{PR} - \mathrm{SU}$.